

Geochemistry, Geophysics, Geosystems

RESEARCH ARTICLE

10.1029/2018GC007868

Key Points:

- Shear wave receiver functions are used to examine the structure of the Pampean flat-slab region
- Results are consistent with the subducting lithosphere both bending and tearing to accommodate the transition to flat-slab subduction
- The migration of flat-slab subduction into the region is cooling the South American lithosphere in the region affecting its viscosity

Supporting Information:

Supporting Information S1

Correspondence to:

R. Porter, ryan.porter@nau.edu

Citation:

Haddon, A., & Porter, R. (2018). S wave receiver function analysis of the Pampean flat-slab region: Evidence for a torn slab. Geochemistry, Geophysics, Geosystems, 19, 4021-4034. https://doi. org/10.1029/2018GC007868

Received 1 AUG 2018 Accepted 11 OCT 2018 Accepted article online 17 OCT 2018 Published online 29 OCT 2018

S-Wave Receiver Function Analysis of the Pampean Flat-Slab **Region: Evidence for a Torn Slab**

A. Haddon^{1,2} and R. Porter¹



¹School of Earth and Sustainability, Northern Arizona University, Flagstaff, AZ, USA, ²Now at Geosyntec Consultants

Abstract Flat-slab subduction is an atypical form of subduction where the downgoing plate assumes a low-angle or subhorizontal geometry as it descends beneath the overriding plate. These systems have profound impacts on upper-plate deformation and volcanism, yet there are outstanding questions regarding the causes, initiation, and termination of flat-slab subduction. The Pampean flat-slab region, located in the South American Cordillera, is an ideal locale to study the evolution of these systems due to its well-constrained geologic history and the continuity of subduction along the western margin of the continent. In this work, we utilize S wave receiver functions (SRFs) to measure the thicknesses and geometry of the subducting Nazca plate lithosphere and the overriding South American plate within the region. Results from this study show overthickened Nazca Plate crust (~15-20 km thick) in the flat-slab region. Prior to the slab steepening, SRFs indicate a velocity increase rather than a decrease at the top of slab crust, which is consistent with a transition from basalt to eclogite within the crust as it dehydrates. Margin parallel cross sections are consistent with differing transitions between flat-subduction and more-typical subduction occurring to the north and south. In the north, the transition appears to be gradual, consistent with slab bending. To the south, SRFs indicate an abrupt change, consistent with slab tearing. These differences are consistent with significant variations in slab rheology along the margin, which may reflect differing thermal regimes. This work has global implications for the three-dimensional effects of flat-slab subduction.

1. Introduction

Flat-slab subduction, an atypical form of subduction where the downgoing plate assumes a subhorizontal or flat geometry, is shown to have a profound impact on upper-plate tectonism. It is commonly associated with upper plate cooling, a shut-off of arc volcanism, and the migration of deformation inboard from the plate margin. Within flat-slab systems, there are outstanding questions regarding the cause of flat-slab subduction and how subducting slabs transition from flat-slab regions to adjacent regions with steeper subduction. The Pampean flat-slab region, located in Chile and Argentina between approximately 29 and 32°S (Figure 1), provides an excellent locale to better understand these processes due to the availability of seismic data and the well-constrained geology of the area. Regionally, flat-slab subduction is commonly attributed to the migration of the Juan Fernández Ridge (JFR) into the area at ~18 Ma (Yáñez et al., 2002). Slab shallowing is associated with an eastward migration of deformation inland from the trench and a shut-off of arc magmatism since the Pliocene (Allmendinger et al., 1990; Jordan et al., 1983; Kay & Abbruzzi, 1996; Kay & Mpodozis, 2002). By applying S wave receiver function (SRF) analysis to this modern flat-slab region, we are able to constrain the slab geometry and improve our understanding of the controls on slab density in flat-slab regions globally.

The Andean Margin is segmented into regions of subhorizontal or flat geometries (i.e., Peru, Chile-Argentina, and Colombia) and regions with more typical subduction geometries of ~30° (Cahill & Isacks, 1992; Gutscher, Maury, et al., 2000; Hayes et al., 2012). Although the effects of flat-slab subduction (e.g., shut off of arc magmatism and migration of deformation away from the trench) are well known, the causes of flat-slab subduction are still debated. Globally, 10% of subduction zones by arc length are characterized as flat-slab or low-angle subduction (Gutscher, Maury, et al., 2000), and their influence on the upper-plate geology is profound (e.g., Dickinson & Snyder, 1978); therefore, a better understanding of this form of subduction is important for understanding global tectonism. This is especially important for evaluating the geologic evolution of the southwestern United States, a region that the Pampean flat-slab region is often considered a modern analogue to (e.g., Jordan et al., 1986).

Many mechanisms have been hypothesized to induce flat-slab subduction. These include (1) subduction of overthickened oceanic crust (i.e., oceanic plateaus or aseismic ridges) resulting in a neutrally buoyant slab

©2018. American Geophysical Union. All Rights Reserved.

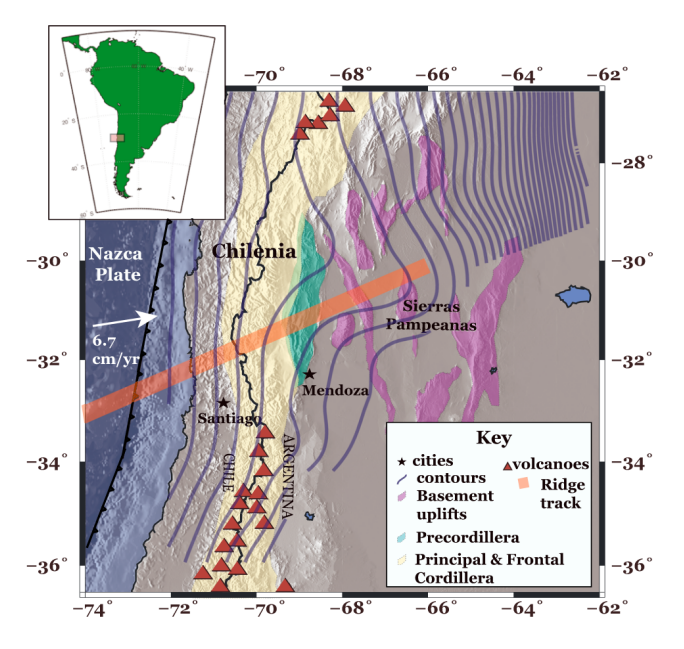


Figure 1. Map of study area including the track of the Juan Fernández Ridge in orange (Yáñez et al., 2001); the modern geological provinces are colored yellow for the High Andes provinces, blue for the Precordillera, and purple for the uplifted basement blocks of the Sierras Pampeanas; active volcanoes are represented by the red triangles; and the contours show the depth of the subducting plate beneath the surface at 20-km intervals (slab 1.0). The map was created using Generic Mapping Tools (Wessel et al., 2013).

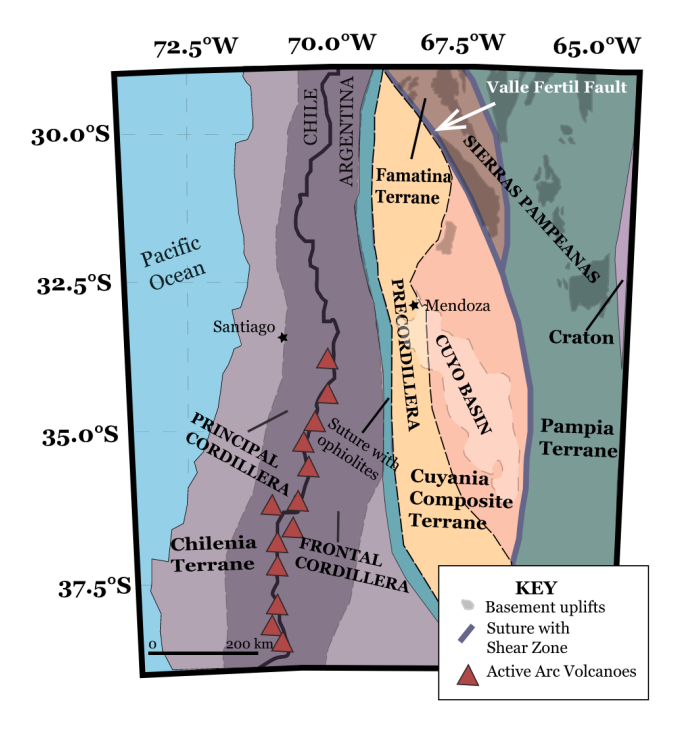


Figure 2. Map of the terranes in the Pampean region in South America. Terranes young to the west. The active volcanic arc is indicated by the regions with red triangles. In the flat-slab region there are no active arc volcanoes. Modified from Ramos (2010).

(especially if the slab crust and slab mantle are hydrated), (2) slab suction due to low pressure zones between the slab and overriding lithosphere, (3) increased trenchward motion of the overriding plate, (4) relatively high subducting plate velocities, and (5) hydration of the downgoing lithosphere (e.g., Cross & Pilger, 1982; Gans et al., 2011; Gutscher, Spakman, et al., 2000; Jischke, 1975; Kopp et al., 2004; Ma & Clayton, 2015; Manea et al., 2011; Manea & Gurnis, 2007; O'Driscoll et al., 2009; Porter et al., 2012; van Hunen et al., 2002b). While it is likely that all of these mechanisms affect subduction angle, identifying one universal cause is difficult, as the relative importance of each likely varies regionally.

Within the study area, the JFR contains zones of overthickened oceanic crust due to volcanism at the Juan Fernández hot spot. Yáñez et al. (2001) estimated that the average crustal thickness of the subducted Nazca plate is ~20–22 km, and Gans et al. (2011) calculated that the oceanic crust is ~14–19 km in the region of flattest subduction. However, Kopp et al. (2004) determined that offshore, sections of the JFR are not overly thickened and have crustal thicknesses of roughly 8–10 km. They instead proposed that buoyancy within the slab is likely a result of hydration in the slab's crust and mantle. It is important to note that crustal thickness along the ridge is likely not uniform (Gans et al., 2011). In this work we utilize SRFs to estimate the crustal and lithospheric thickness within the Pampean region for both the overriding South American lithosphere and the subducting Nazca plate to better understand their effects on subduction angle.

2. Background

2.1. Regional Geological Setting

The Andean margin is an N-S striking orogenic belt that formed from the subduction of the Nazca plate beneath the western margin of the South American continent. Along the strike of the Andean margin, there are variations in subduction style, lithospheric structure and thickness, style of deformation, and volcanic activity. Given the relatively consistent age of the subducting plate and the convergence rate, the Andean margin provides an excellent locale to better understand the factors that control the evolution of convergent orogenic belts. One of the primary factors thought to influence this orogenic behavior within the Andean margin is the angle of subduction.

Within the study area, the South American continent consists of an amalgamation of parautochthonous and allochthonous terranes that young to the west and were accreted to the Rio de Plata craton starting in the Mesoproterozoic (Figure 2). This includes (from east to west) the Pampia terrane, the Famatina terrane, the Cuyania Composite terrane, and the Chilenia terrane. The present-day geology of the Pampean region is influenced by preexisting structures within these accreted terranes and previous accretion and extensional events. Modern geologic provinces from west to east are the Principal Cordillera, Frontal Cordillera, Precordillera, and Sierras Pampeanas (Figure 1).

The High Andes are located within the Chilenia terrane and can by subdivided into the Principal Cordillera located to the west and Frontal Cordillera to the east, although the boundary between the two is not well constrained due to volcanic cover (Ramos et al., 2002). The Precordillera lies to the east of the Andes on the Cuyania terrane and is characterized



as a thin-skinned thrust belt with four to six major west-dipping thrust faults (Allmendinger et al., 1990). Basement rocks in the Precordillera are composed of Paleozoic shelf carbonates (Astini et al., 1995). The Precordillera accounts for ~65–70% of the shortening in this region of the Andes since ~10 Ma (Allmendinger et al., 1990). The eastern portion of the Cuyania terrane extends into the Sierras Pampeanas, which is a thick-skinned deformation belt that extends from the Precordillera to the western margin of the Rio de Plata Craton and includes the Pampia Terrane (Figures 1 and 2). Deformation and uplift of the Sierras Pampeanas is a result of compression during the late Cenozoic and is thought to be correlated to the onset of flat-slab subduction. The mountains, composed of crystalline basement rock, were uplifted by reverse faulting often along reactivated normal faults (Ramos et al., 2002).

2.2. Global Controls on Subduction Angle

The age of the descending oceanic lithosphere and rapid convergence rates are likely important factors for influencing the angle of subduction in a global context. Though it is unlikely these mechanisms are the primary driving mechanism in the Pampean region, they likely play a broad role in controlling subduction angle and can explain the differences in subduction styles between the eastern and western Pacific (e.g., Uyeda & Kanamori, 1979).

Due to differing thermal conditions, young oceanic lithosphere has a lower density than older oceanic lithosphere. In regions where some of the steepest subduction is occurring globally (e.g., Marianas), the age of the oceanic lithosphere is much older than most of the regions where flat-slab subduction is actively occurring (Hayes et al., 2012; Müller et al., 2008; Stern, 2002). In South America, age is relatively constant along the length of the Andean Margin and there is no correlation with age and flat-slab regions (Pilger, 1981). The youngest ages of the Nazca plate at the trench are near the triple junction of the Chile Ridge, the most southern boundary of the Nazca plate, and ages increase northward from that location (Müller et al., 2008). Although the age of the plate may play a role in predicting where flat-slab subduction is more likely to occur, other mechanisms are required to explain the multiple flat-slab regions in South America.

Increased upper plate motion has also been proposed as a mechanism for driving flat-slab subduction. Geodynamic modeling by Manea et al. (2011) demonstrates that flat-slab subduction is more likely to occur in regions where the continental plate is overriding the trench at a relatively fast rate. Convergence rates along the entire Andean margin are relatively rapid at a rate of ~7 cm/yr, which is fairly consistent along the entire subduction zone (DeMets et al., 2010). The Andean margin exhibits relatively low-angles of subduction, which may result from this rapid convergence. However, flat-slab subduction is not characteristic of the entire margin, and, as such, it is unlikely that rapid overriding plate motion is the only factor driving flat-slab subduction within the region. Along strike variations of subduction angles and deformation are likely related to variations in the structure and composition of the overriding and downgoing plates (Cloos, 1993; Kay & Mpodozis, 2002).

2.3. Local Influences on Slab Geometry in the Pampean Region

Overthickened oceanic crust found at aseismic ridges or seamounts has been proposed as potential cause of flat-slab subduction (e.g., Jordan et al., 1986). This hypothesis is based on the idea that thickening oceanic crust lowers the mean density of the downgoing lithosphere and, if the crust is thick enough, it can result in a neutrally buoyant slab. In the Pampean flat-slab region, the shallowest subduction correlates with the track of the subducted JFR, a seamount chain formed at the Juan Fernández hot spot (Anderson et al., 2007; Barazangi & Isacks, 1976; Yáñez et al., 2001). Additionally, for island seamount chains, like the JFR, the age of the crust is younger than the surrounding oceanic crust, which likely reduces slab density due to thermal expansion of the oceanic lithosphere (Pilger, 1981).

Slab suction forces can induce low-angle subduction in regions where thick lithosphere is present in the overriding plate. Slab suction is the result of a negative pressure within the mantle wedge that forms when the subducting slab and overriding lithosphere are in close proximity. This process pulls the subducting slab upward rather than allowing it to descend into the mantle (O'Driscoll et al., 2009) and is controlled by subduction velocity, thickness, and viscosity of the mantle wedge and varying thickness of the overriding lithosphere. Lower viscosity asthenosphere can decrease the magnitude of suction (Manea & Gurnis, 2007). In areas where the root of a craton is present, corner flow within the mantle wedge can be impeded and potentially increase the negative pressure above the descending slab pulling it into a flat geometry (Manea et al.,



2011). In models from O'Driscoll et al. (2009), regions with 250-km-thick cratonic roots that are located within ~300 km from the trench exhibit almost double the suction forces than those without deep roots. Given the proximity of the Rio de La Plate Craton to the margin (Figure 2), this is a potential driver of flat-slab subduction within the Pampean region.

In typical subduction zones, the transition from basalt to eclogite is expected to occur within the downgoing oceanic crust at depths of 80–100 km. This reaction should increase the overall density of the downgoing slab due to the growth of high-density garnets that replace lower-density phases (Hacker et al., 2003). For oceanic crust with a common thickness of 7 km, the crust is expected to convert to eclogite in this depth range and become negatively buoyant (van Hunen et al., 2002a). However, thickened crust may provide enough buoyancy to induce flat-slab subduction and delay this transition to eclogite because slab flattening results in a cooler thermal structure of the closely coupled plates (English et al., 2003; Gutscher, 2002; van Hunen et al., 2004).

Slab hydration may also contribute to the buoyancy of the oceanic lithosphere. Hydration of the slab mantle will increase its buoyancy by converting dense olivine to low-density hydrous phases such as serpentinite (Kopp et al., 2004; Porter et al., 2012). Within the Pampean region, a ~5% percent serpentinization of the subducting mantle lithosphere would lower the slab density enough to make it neutrally buoyant (Porter et al., 2012). Increased slab hydration due to hydrothermal activity associated with hot spot volcanism could lower the density of slabs along aseismic ridges relative to adjacent oceanic lithosphere.

2.4. Evolution the Pampean Flat Slab

There is a consensus among most researchers that flat-slab subduction in the Pampean region is likely associated with the subduction of the JFR. This is primarily based on the spatial correlation between the hot spot track and the region of flattest subduction and the temporal correlation between ridge migration into the region and the onset of flat-slab subduction (Pilger, 1981; Yáñez et al., 2001). This correlation may be due to the JFR's thickened oceanic crust or increased hydration providing the buoyancy necessary to maintain flat-slab subduction (Gans et al., 2011; Kopp et al., 2004; Porter et al., 2012).

Subduction of the JFR likely began at ~18 Ma and the ridge intersected the trench at 33°S at ~11 Ma (Yáñez et al., 2002). Geologic evidence shows that at 20 Ma, the Principal Cordillera had not yet been affected by the collision of the JFR (Ramos et al., 2002). The first evidence of the onset of flat-slab subduction in the upper plate is the volcanic arc advancing eastward from ~14 to 9 Ma (Kay & Abbruzzi, 1996). This eastward migration continued from ~9 to 6 Ma when arc volcanism was concentrated in the Sierras Pampeanas (Ramos et al., 2002). Arc magmatism is recorded in the eastern most Sierras Pampeanas during the Pliocene until cessation at 1.9 Ma (Kay & Abbruzzi, 1996; Kay & Mpodozis, 2002). The timing of this arc migration also coincides with the uplift of the Precordillera, the end of thin-skinned contraction in Principal Cordillera, and the uplift of Frontal Cordillera (Ramos et al., 2002).

3. Methods

S-wave receiver functions are an effective technique for locating major velocity contrasts, such as the lithosphere-asthenosphere boundary (LAB), in regions where the lithospheric structure is complex, like the Pampean flat-slab region (Heit et al., 2008). In traditional P-wave receiver functions, the P wave to S wave (Ps) conversion can be obscured by arrivals known as multiples, which are recorded at the receiver and undergo multiple reflections off of the Earth's surface and a subsurface interface during travel. The SRF method is less likely to be complicated by the arrival of multiples because the S wave to P wave converted (Sp) phase, which forms at an impedance contrast within the Earth, traverses a different path within the crust and upper mantle and the converted P wave arrives at the receiver prior to the multiples (Heit et al., 2008; Lekić & Fischer, 2014). Additionally, the frequency content of S to P converted phases is much lower than that of P to S converted phases; therefore, it has a lower spatial resolution and is ideal for studying gradual discontinues such as the LAB. The SRF method has successfully been used for mapping the Moho and upper-mantle discontinues such as the LAB (e.g., Abt et al., 2010; Farra & Vinnik, 2000; Lekić & Fischer, 2014; Liu & Gao, 2018; Wilson et al., 2006; Yuan et al., 2006).

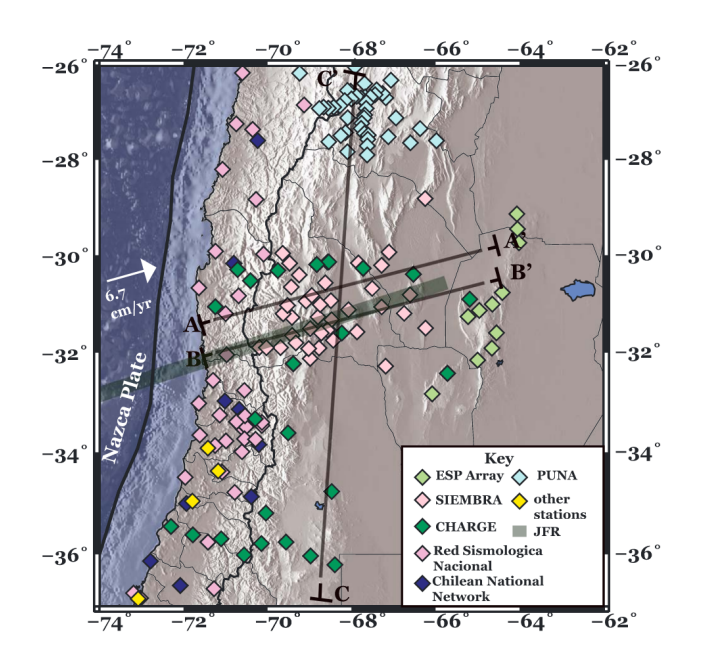


Figure 3. Map of networks and individual stations used for this project. Lines A-A', B-B', and C-C' show the locations of the cross sections shown in Figures 4–6. The opaque orange line shows the track of the Juan Fernández Ridge. Map made using Generic Mapping Tools (Wessel et al., 2013).

3.1. Data Processing

Earthquake data were acquired from the IRIS (Incorporated Research Institutions for Seismology) Data Management Center for publicly available three component broadband seismometers located within the Pampean flat-slab region and surrounding areas. A total of 200 stations from the following networks: Chilean National Network, ESP Array, SIMEBRA Array, and CHARGE experiment were analyzed (Figure 3). Events with an $M_{\rm w}>5.8$ from epicentral distances of 55° to 85° were selected to ensure clear arrivals, to minimize the contamination of the S to P converted signals with other converted signal arrivals and reverberations, and to avoid any effects of postcritical S waves.

The, three component data were filtered between 0.1 and 0.75 Hz and rotated to the SH-SV-P coordinate system (Hansen & Dueker, 2009; Kumar et al., 2005; Li et al., 2004), by using the free-surface transfer matrix (Kennett & Engdahl, 1991):

where α is near surface compressional velocities, β is near surface shear velocities, $\mathbf{q}_{\alpha} = (\alpha^{-2} - \mathbf{p}^{2})^{0.5}$, $\mathbf{q}_{\beta} = (\beta^{-2} - \mathbf{p}^{2})^{0.5}$, and p is the ray parameter of the direct phase. We solve for Vp and Vp/Vs as in Abt et al. (2010)

Deconvolution was accomplished using an extended time multitaper deconvolution initially introduced by Park and Levin (2000) and modified by Helffrich (2006). For this study, a time bandwidth product of 4 was used with 3 Slepian tapers based on the recommendation of Shibutani et al. (2008) and implementation of Lekić and Fischer (2014). The multitaper deconvolution was developed to address the problem of separating actual signal from signal generated noise, which is generally difficult to do because the receiver function analysis is composed on scattered waves and multiple reverberations (Park & Levin, 2000). The method is similar to spectral division; however, it uses several multitaper correlations to estimate frequency domain RFs in order to avoid instabilities in spectral division (Ammon et al., 1990; Park & Levin, 2000). The multitaper spectrum is resistant to noise because it minimizes spectral leakage and preserves phase information from the signal by using a sequence of tapers that are used to window the time series for its full length and then summing individual signals that have been converted into the frequency domain through a Fourier transformation.

Common-conversion point stacking was utilized to migrate receiver functions to depth. CCP stacking weights the mean of the amplitudes of each receiver functions that traverses a bin in the subsurface (Dueker & Sheehan, 1997). SRFs were migrated to depth using the IASP91 velocity model (Kennett & Engdahl, 1991), and postcritical arrivals were removed. SRFs were projected along their incoming raypaths and separated into 50-km bins. The amplitude at each grid point was calculated by averaging data from 1.25 bins away. These values were chosen based on visual inspection of the CCP stacks. Smoothing the data enhances the signals laterally by closing gaps in ray coverage. Based on visual inspection of the traces, RF traces with maximum absolute values of amplitude greater than 0.6 were deemed unrepresentative of lithospheric structure and removed.

3.2. Resolution and Error Analysis

While the station coverage across the Pampean flat-slab region allows for the calculation of a relatively high-resolution CCP model, there are areas where the coverage is less than ideal. Figure S1 in the supporting information shows the number of raypaths sampling each bin for the cross sections presented in this manuscript.

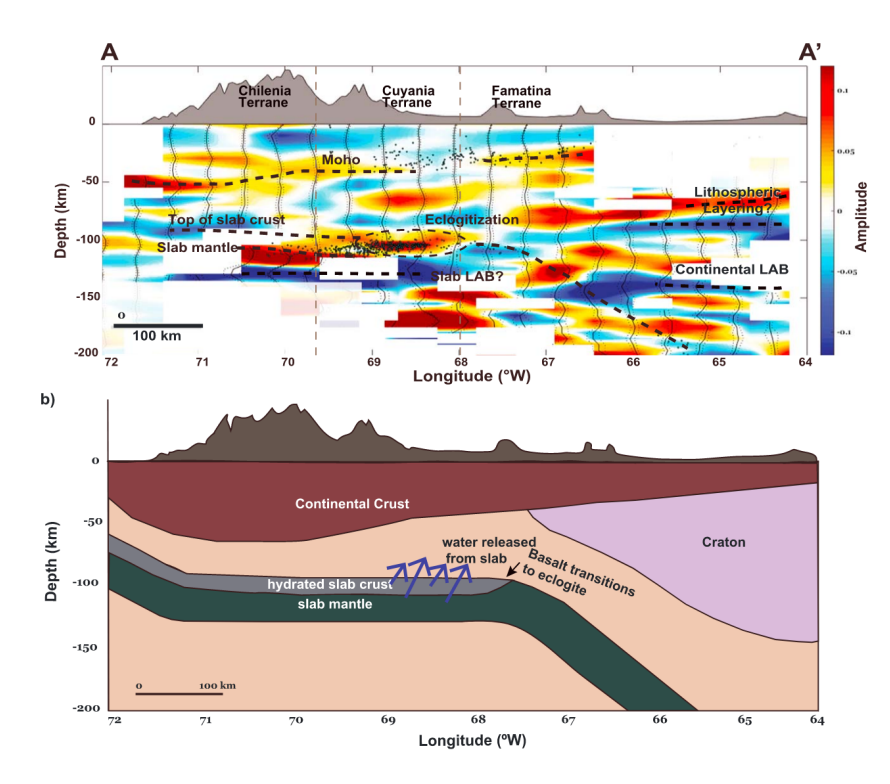


Figure 4. (top) Interpreted CCP *S* wave receiver function cross section A-A'. The dashed vertical lines show standard deviations, and the grayed out regions denote areas of insufficient ray coverage for an interpretation. (bottom) Cartoon of interpreted cross section showing the location of the basalt-to eclogite transition. Earthquake locations are from Linkimer (2011). Topography has 40× vertical exaggeration.

To assess error, we perform a bootstrapping analysis of our CCP stacks. Forty bootstrap iterations were performed at each grid point in the model. For each iteration, a random subset of traces was selected and the mean value calculated. The mean values of the iterations at each grid point are shown in our results, and the error is estimated as the standard deviation of the bootstrapping analysis. This is shown as the dashed lines in cross section A-A', B-B', and C-C', and cross sections of standard deviation are shown in Figure S2. Based on these estimates of error and ray coverage, we focus our analysis and discussion on well-sampled regions with low standard deviations.

4. Results

CCP stacks of the SRFs were calculated for the Pampean flat-slab region parallel to the track of the Juan Fernandez Ridge and parallel to the trench (Figure 3). Amplitudes were multiplied by -1 so that SRF results are consistent with PRF analyses. In the discussion below, an increase in the velocity of a seismic wave at a boundary within the Earth is represented by a positive amplitude, whereas decreases at a boundary within the Earth are represented as negative amplitudes.

4.1. Structure of the South American Lithosphere

Figures 4 and 5 show the ridge-parallel CCP cross sections calculated for the flat-slab region. Within the cross section, the Moho is interpreted as a strong positive arrival that is imaged at a maximum depth of \sim 65 km beneath the High Andes in the western part of the study area and a minimum depth of \sim 35 km to the east beneath the Sierras Pampeanas (Figures 4 and 5). In Figure 4 (A-A'), the depth change in the Moho is more gradual across this boundary. West of -71° W, the Moho signal is difficult to interpret due to reduced resolution in this region.

East of -66° W, a negative amplitude arrival is present in all ridge-parallel cross sections at a depth of ~125 km. This is interpreted as the base of the cratonic lithosphere to the east of the flat-slab region (Figures 4 and 5). The base of the craton has also been imaged by a previous SRF study within the region (Heit et al., 2008) and in a shear wave velocity model calculated from surface waves (Porter et al., 2012).

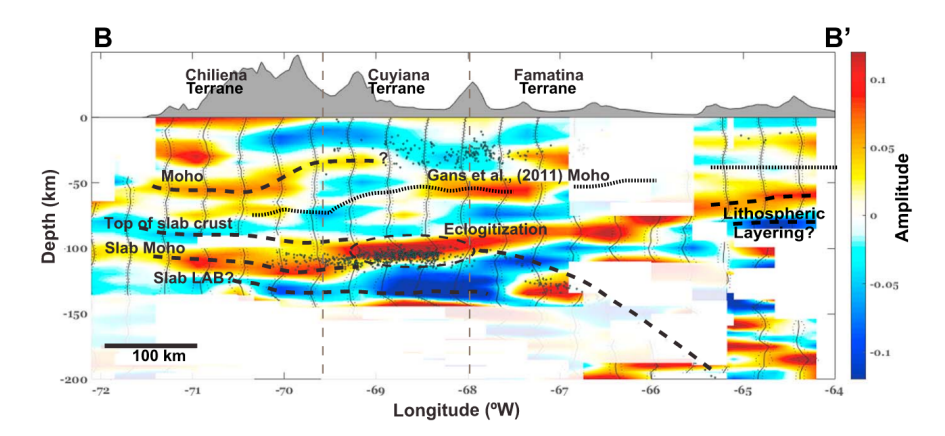


Figure 5. Interpreted CCP *S* wave receiver function cross-section B-B'. The dashed black lines indicate the locations of the Moho, the top of slab crust, the slab Moho, slab LAB, and the Moho interpreted by Gans et al. (2011). Terrane boundaries are represented as dashed gray lines. The black dots are earthquake locations from Linkimer (2011). Topography has 40× vertical exaggeration. The dashed vertical lines show standard deviations, and the grayed out regions denote areas of insufficient ray coverage for an interpretation.

Our results agree with those estimates of LAB depth. In cross-sections A-A' and B-B' we also image a positive and negative pair of arrivals in the lithosphere labeled lithospheric layering in Figures 4 and 5. These arrivals are commonly observed in cratonic lithosphere and may be indicative of metasomatism or variations in the orientation of seismic anisotropy (Abt et al., 2010; Ford et al., 2016; Hansen et al., 2015; Wirth & Long, 2014).

4.2. Structure of the Nazca Plate

In the western part of the study area, a negative conversion at a depth of \sim 90–95 km is followed immediately by a positive conversion at \sim 110 km depth (Figures 4 and 5). These arrivals are interpreted as the top of the slab crust and slab Moho, respectively. This agrees with work by Gans et al. (2011), who also identify the negative-positive phase change as the slab crust and mantle. The basaltic crust and pelagic sediments making up the slab-crust are expected to produce a negative conversion because they exhibit lower seismic velocities than the overlying lithospheric mantle. The top of the slab mantle (Moho) is the positive amplitude arrival located just after the negative amplitude as the velocity increases from the slab-crust to the underlying slab mantle. The interpretation of these features as the top and bottom of the slab crust was also informed by slab seismicity at \sim 100–110 km depth (Figures 4 and 5), which is thought to result from dehydration embrit-tlement as hydrous phases become unstable and the slab dewaters. Based on these arrivals, the thickness of the slab crust is interpreted to be \sim 15–20 km within the region.

This negative-positive pair of arrivals is imaged clearly in the cross section west of -69° W and correlates well with regional seismicity (Linkimer, 2011). East of -69° W, the negative amplitude, interpreted as the top of the slab crust, changes to a positive amplitude arrival. Gans et al. (2011) also noted this transition and hypothesize that it could indicate that the slab transitioned to eclogite, which is consistent with our results. At -67° W slab seismicity shows a change in geometry to a steeper angle of subduction (Anderson et al., 2007; Linkimer, 2011). Steeply dipping features cannot be imaged clearly by receiver functions, which is likely why the top of the slab is not imaged clearly in this region.

In Figures 4 and 5 a negative arrival is observed at a depth of ~150 km that persists for the length of the flatslab until it resumes a steeper angle of subduction. This arrival is interpreted as the base of the downgoing oceanic plate, which is expected to produce a decrease in seismic velocity with depth. In the transects A-A' and B-B' the thickness of the subducting Nazca plate (top of the subducting slab to the slab LAB) appears to be ~55–65 km (Figures 4 and 5). The negative amplitude arrival interpreted as the top of the basaltic oceanic crust and the negative arrival interpreted as the slab LAB are used to infer this thickness.

Figure 6 shows a trench parallel cross section of the Andean Margin from 26°S to 37°S. The flat-slab region is located between roughly 32°S and 29°S. In Figure 6, the crust and mantle of the flat-slab (negative-positive amplitude change) are located at a depth of roughly 100 and 120 km, respectively. North of 29°S there is a continuous but slight bend in the negative-positive amplitude and the depth increases from ~120 to

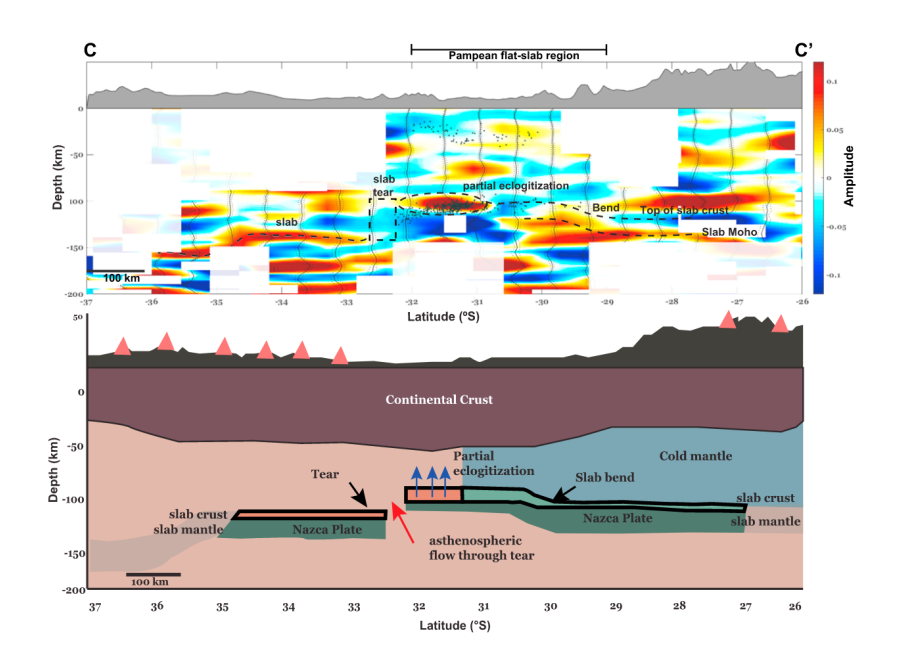


Figure 6. (top) Interpreted CCP *S* wave receiver function cross-section C-C'. (bottom) Cartoon of cross section showing the interpreted slab tear, asthenosphere moving through tear to partially eclogitized slab curst in flat-slab segment. Note the cold mantle trailing behind the flat-slab segment from north to south. Earthquake locations are from Linkimer (2011). Topography has 40× vertical exaggeration. The dashed vertical lines show standard deviations, and the grayed out regions denote areas of insufficient ray coverage for an interpretation.

~130 km (Figure 6). Between 31°S and 32°S, the signal interpreted as the top of the slab crust at ~100 km is not imaged. Seismicity plotted on the cross section increases in depth where the top of the slab is no longer imaged.

5. Discussion

5.1. Upper Plate Structure

The South American Moho signal is identified as a strong positive amplitude arrival observed in the E-W cross sections east of 67°W (Figures 4 and 5). Calculated Moho depths for the South American plate agree with previous results that show thick crust (~65 km) beneath the High Andes that thins to the east beneath the Sierras Pampeanas. Moho depths within the Sierras Pampeans are ~45–55 km and potentially as shallow as 35 km (Ammirati et al., 2013, 2015, 2016; Fromm et al., 2004; Gilbert et al., 2006). These Moho depth estimates beneath the High Andes are slightly less than estimates from Gans et al. (2011) and Heit et al. (2008) of ~70 km. This may reflect differences in the most prominent positive conversion in the different profiles. In Figure 5, which most closely aligns with the Gans et al. (2011) profile, we observe a weak positive arrival that agrees well with their Moho. This may be evidence for eclogitization of the lower crust in the region, which could produce multiple positive conversions within the crust.

West of 70°W, the continental Moho seismic discontinuity is not easily identifiable, which is consistent with previous receiver function studies of this region (Gilbert et al., 2006; Heit et al., 2008). Gilbert et al. (2006) argue that in the regions of thickest crust beneath the high Andes, the lower crustal material may have transformed into eclogite due to the pressure-temperature conditions at that depth. Eclogitization would lead to an increase in lower-crustal seismic velocities, which would reduce the amplitude of conversions from the Moho velocity discontinuity. Local receiver functions calculated by Ammirati et al. (2016) show that the Moho is observed as two smaller conversions at 60–65 km and 50–55 km and argue that this can be used to distinguish regions where the crust has been converted to eclogite. In a previous SRF study, Heit et al. (2008) observed a negative phase at ~71°W at a depth of ~50 km that they identified as the Moho. They suggested that the positive phase typically identified as the Moho changes to a negative phase in this area due to hydration and serpentinization of the fore-arc mantle wedge, which can reduce the seismic velocities. In



Cascadia this hydration resulted in an "inverted" Moho signal in receiver functions, due to the decreases in seismic velocity at this interface (Bostock et al., 2002).

Moho depth variations in the Pampean flat-slab region correspond to terrane boundaries and recent tectonic boundaries. In Figures 4 and 5 there is a change in crustal thickness at 69°W that correlates particularly well with the boundary between the Chilenia and Cuyania terranes and another at 67.5°W that correlates with the boundary between the Cuyania and Famatina terranes. Ammirati et al. (2016) proposed the presence of a major structure separating these two boundaries that they constrained with crustal seismicity and focal mechanisms.

The base of the South American lithosphere is observed within the study area east of 67°W in Figures 4 and 5 as a negative arrival. This negative arrival increases in depth to the east and is interpreted as the bases of the cratonic lithosphere of the Rio de la Plata Craton. The LAB reaches a maximum depth of ~150 km in these figures. Estimates of LAB depth in Figures 4 and 5 are consistent with previous SRF, gravity, and shear wave models (Heit et al., 2008; Porter et al., 2012; Tassara et al., 2006; Tassara & Echaurren, 2012). In the western portion of the study area, where the slab is nearly horizontal, a clear LAB is not imaged. This is possibly because the subducted Nazca plate is in close enough proximity to the overriding plate that its base cannot be differentiated from the top of the flat-slab. It is also possible that mantle lithosphere was removed in this region by the flat Nazca slab.

The lithospheric root of the Rio de la Plate craton imaged by the SRFs is in relatively close proximity to the trench (~600 km; Figure 4). As such, it is probable that this cratonic root is impeding mantle corner flow in this region. This process is expected to produce a zone of decreased pressure, or slab suction, above the subducting slab and may help induce flat-slab subduction (Manea et al., 2011; O'Driscoll et al., 2009; van Hunen et al., 2004). Slab suction has been proposed in regions where flat-slab subduction actively occurs in proximity to cratonic roots. Manea et al. (2011) modeled that slab-suction in combination with trenchward motion of the cratonic lithosphere and trench retreat were enough to induce flat-slab subduction. However, this work also showed that without trench ward motion of the cratonic lithosphere, slab-suction alone would not be enough to induce flat-slab subduction (Manea et al., 2011).

Slab suction is unlikely to be the sole driver of flat-slab subduction as slab flattening does not occur in all areas where a cratonic root is present (van Hunen et al., 2004). Additionally, flat-slab subduction is commonly associated with aseismic ridges (Gutscher, Maury, et al., 2000) and oceanic plateaus (Liu et al., 2010). However, the proximity of the trench to the craton in the Pampean flat-slab region suggests that slab suction likely played a role in the onset of low angle subduction within the region in addition to other factors.

5.2. Subducting Plate Structure

The negative-positive amplitude pairs at ~90–95 km and ~110 km are interpreted in cross sections in Figures 4 and 5 as the top and bottom of the subducting Nazca plate crust, respectively. The thickness of the subducting crust varies slightly in all the cross sections shown in Figures 4 and 5. van Hunen et al. (2002a) found that an overthickened oceanic plateau or aseismic ridge with a thickness of ~13–14 km has enough buoyancy to support flat-slab subduction. Regional work found that a minimum crustal thickness of 13 km provides enough buoyancy to support a slab that is 40–50 Ma with a total thickness of 70–80 km (Gans et al., 2011).

In Figure 4, there are slight variations in the vertical distance between the negative-positive pairs in the cross section. These variations may be a result of faulting that occurred offshore prior to the subduction of the Nazca plate (Fromm et al., 2006; Gans et al., 2011). Displacement may be due to fault reactivation during slab bending that offsets the whole slab crust. Alternately, this observation may indicate that the JFR thickness varies across the region. The offshore segments of the JFR exhibit evidence of variable volcanic activity, and it is likely that this is true for the subducted segments as well. Variations in crustal thickness may reflect this nonuniform volcanic activity and associated nonuniform crustal thickening.

At ~150 km depth, there is a persistent negative arrival that is interpreted as the slab LAB. East of 67°W, this phase is no longer present, similar to the slab crust and mantle signals. This is likely because the slab has assumed a steeper angle of subduction making it difficult to image with receiver functions. Based on this interpretation, we calculated a total slab thickness of ~55–65 km. This thickness estimate agrees with

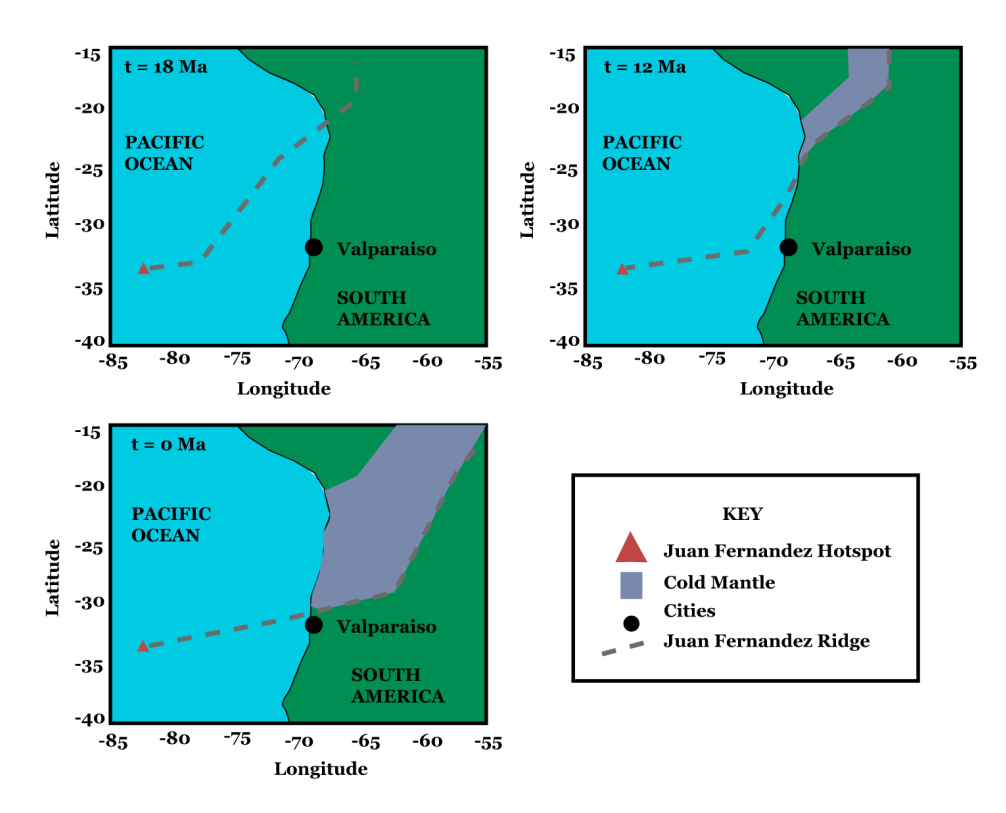


Figure 7. Migration of the Juan Fernández Ridge from 18 Ma to present. The purple region represents the mantle that cooled above the flat-slab as it migrated southward over time. The cold mantle above the flat-slab remained cold after the ridge migrated through that region. Modified from Yáñez et al. (2002).

estimates of oceanic lithosphere for the Pacific basin calculated by Leeds (1975) and with previous estimates for the region (Gans et al., 2011).

5.3. Slab Eclogitization

Before the slab resumes a steeper angle of subduction ~600 km inboard from the trench, the negative-positive phase changes interpreted as the slab crust and slab mantle, respectively, are no longer imaged (Figure 4). A similar pattern is observed in *P* wave receiver functions, which is interpreted as evidence for slab eclogitization in the eastern part of the study area (Gans et al., 2011). Eclogitization would reduce the velocity contrast between mantle peridotite and the slab crust that would result in the absence of a converted phase from this boundary. It is interesting to note that at 68°W, the negative arrival interpreted as the top of the slab crust is no longer imaged and is replaced with a positive amplitude arrival (Figure 4). This positive amplitude indicates an increase in velocity with depth and may represent the top of the eclogitized slab crust. This observation is consistent with ecologitization occurring at this location. This phase change would increase slab density and may be driving the change in subduction angle that also begins at this location. Porter et al. (2012) observed a low velocity zone between the continental LAB and the subducted slab after it assumes a more typical angle of subduction. They interpret this zone as serpentinized mantle or hydrated continental lithosphere. The positive amplitude arrival in our CCP images may represent the transition between the bottom of this layer and the top of eclogitized oceanic crust.

5.4. Along-Strike Variations in Slab Geometry

To accommodate the along-strike variations in subducting geometry, the subducting Nazca plate must either bend or tear (Phillips & Clayton, 2014; Scire et al., 2015). In the N-S striking cross section in Figure 6, the slab appears to bend to the north of the flat-slab region to accommodate this change in slab-dip from flat to a more typical angle. The negative-positive pair interpreted as the slab crust and slab mantle begin to increase in depth gradually from 100 km to roughly 120 km to the north. This pair of arrivals persists down to 120 km, which is deeper than the stability field for uneclogitized basalt. However, the phase change to eclogite may

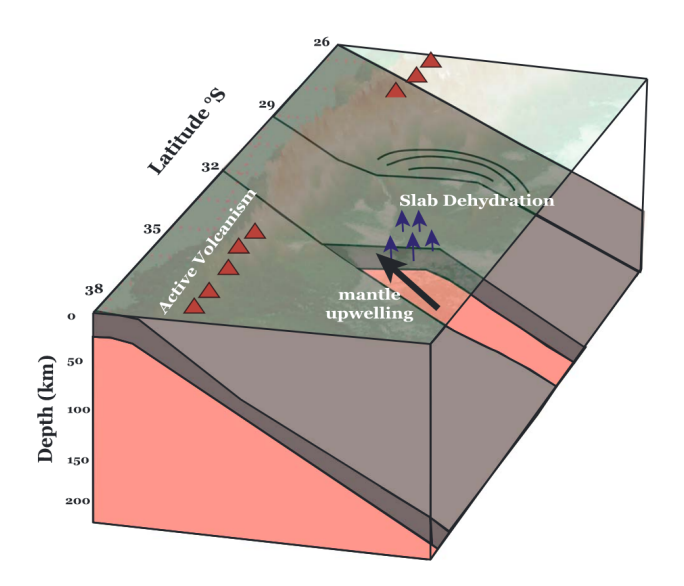


Figure 8. Block diagram showing the modern slab geometry and the location of slab tearing. This tearing allows for asthenopsheric upwelling that heats and partially eclogitizes the slab crust in its vicinity. North of the tear, the upper plate is refrigerated due to the migration of the flat slab through the region. This results in cold conditions at the top of the slab, which prevents eclogitization from occurring. South of the tear, normal subduction and an active volcanic arc are observed.

be delayed by a cooler thermal structure of the slab in that region. This could potentially be a result of the flat-slab migrating into the region from the north and cooling the overlying mantle as it passed through (Figure 7). If cooler mantle conditions are present in this region, it is expected to increase mantle viscosities, which would enhance slab suction and may help explain the gradual increase in slab angle to the north.

At ~32°S, the negative arrival interpreted as the top of the oceanic crust disappears abruptly to the south and is replaced by an anomalous positive amplitude at a depth of 100 km (Figure 6). Immediately south of this, a positive arrival is observed at 150 km depth and is interpreted as the top of the eclogitized slab. The lateral juxtaposition of these negative and positive arrivals is interpreted as evidence for the eclogitization of oceanic crust possibly due to warming associated with a slab tear. The offset of the positive reflector is interpreted as evidence for a slab tear. Slab tearing would allow for hot asthenosphere to flow upward through the tear, which would warm the southern edge of the flat slab in this region. Increased temperatures could induce slab dehydration and enable eclogitization of the basaltic crust adjacent to the tear (Figure 8).

Our hypothesized tear is consistent with previous work that identified a slab hole downdip of our proposed tear (Lynner et al., 2017; Portner et al., 2017). The slab hole can be explained by two end-member hypotheses. The first is that slab deformation and tearing is a result of material upwelling beneath the subducting slab (Burd et al., 2013; Portner et al., 2017). This explanation has been invoked to explain a hole in the Juan

de Fuca slab resulting from the rising plume beneath Yellowstone hot spot in the western United States (Obrebski et al., 2010). Magnetotellurics studies in the region suggest that there is a mantle plume extending from the top of the transition zone (410 km) to the base of the lithosphere. Montelli et al. (2006) and French and Romanowicz (2015) argued that mantle plumes likely originate deep within the mantle and there is no evidence for this in the Pampean region. The other explanation is that the slab hole is a result of tearing due to buoyancy contrasts between the two slab segments. The tear allows the underlying mantle to flow through into the overlying mantle wedge. Buoyancy contrasts within the crust have been used to explain tearing in subducting slabs that have crustal thickness variations (Gutscher, Spakman, et al., 2000; Hu & Liu, 2016).

6. Conclusions

S-wave receiver function imaging of the Pampean flat-slab region are consistent with the hypotheses that overthickened crust, delays in the basalt-to-eclogite transition, and slab suction all play a role in initiating flat-slab subduction. CCP images parallel to the subducting Juan Fernandez Ridge show that prior to the slab resuming a more typical angle of subduction, eclogitization occurs after the slab dewaters. This implies that the slab is hydrated while assuming a flat geometry. Within the region, variations in slab dip are accommodated by downward bending of the flat-slab to the north and tearing of the slab to the south. Tearing is potentially causing partial eclogitization of the slab crust from upwelling asthenosphere adjacent to the tear, which would increase its density and may produce the dip in seismicity observed at the southern edge of the flat-slab (Figure 8). These variations in the transition from flat- to typical-angle slab geometries may have a profound influence on the thermal regime of the region, with cooler overriding lithosphere present in the regions to the north where the slab was previous flat (Figure 7). This variation in temperature would influence the overriding mantle viscosity and may lead to a delay in renewed volcanic-arc activity following flat-slab subduction.

We acknowledge Ved Lekic, who provided the receiver function code for this work; the University of Arizona GSAT group for data collection; and IRIS for data archival. Reviews from Karen Fischer and Alex Nikulin greatly improved the quality of the manuscript. All data are available from the IRIS Data Management Center (https://ds.iris.edu/ds/nodes/dmc/). This work was funded by Northern Arizona University and NSF Award EAR-1645227.

Acknowledgments

References

Abt, D. L., Fischer, K. M., French, S. W., Ford, H. A., Yuan, H., & Romanowicz, B. (2010). North American lithospheric discontinuity structure imaged by Psand Spreceiver functions. *Journal of Geophysical Research*, 115, B09301. https://doi.org/10.1029/2009JB006914



- Allmendinger, R. W., Allmendinger, R. W., Figueroa, D., Snyder, D., Beer, J., Mpodozis, C., et al. (1990). Foreland shortening and crustal balancing in the Andes at 30 S latitude. *Tectonics*, 9, 789–809. https://doi.org/10.1029/TC009i004p00789
- Ammirati, J. B., Alvarado, P., & Beck, S. (2015). A lithospheric velocity model for the flat slab region of Argentina from joint inversion of Rayleigh wave phase velocity dispersion and teleseismic receiver functions. *Geophysical Journal International*, 202(1), 224–241. https://doi.org/10.1093/gji/ggv140
- Ammirati, J. B., Alvarado, P., Perarnau, M., Saez, M., & Monsalvo, G. (2013). Crustal structure of the Central Precordillera of San Juan, Argentina (31°S) using teleseismic receiver functions. *Journal of South American Earth Sciences*, 46(c), 100–109. https://doi.org/10.1016/j. isames.2013.05.007
- Ammirati, J. B., Luján, S. P., Alvarado, P., Beck, S., Rocher, S., & Zandt, G. (2016). High-resolution images above the Pampean flat slab of Argentina (31–32°S) from local receiver functions: Implications on regional tectonics. *Earth and Planetary Science Letters*, 450(C), 29–39. https://doi.org/10.1016/j.epsl.2016.06.018
- Ammon, C. J., Randall, G. E., & Zandt, G. (1990). On the nonuniqueness of receiver function inversions. *Journal of Geophysical Research*, 95, 15,303–15,318. https://doi.org/10.1029/JB095iB10p15303
- Anderson, M., Alvarado, P., Alvarado, P. M., Zandt, G., & Beck, S. (2007). Geometry and brittle deformation of the subducting Nazca Plate, Central Chile and Argentina. *Geophysical Journal International*. 171(1), 419–434. https://doi.org/10.1111/i.1365-246X.2007.03483.x
- Astini, R. A., Benedetto, J. L., & Vaccari, N. E. (1995). The early Paleozoic evolution of the Argentine Precordillera as a Laurentian rifted, drifted, and collided terrane: A geodynamic model. *Geological Society of America Bulletin*, 107(3), 253–0273. https://doi.org/10.1130/0016-7606(1995)107<0253:TEPEOT>2.3.CO;2
- Barazangi, M., & Isacks, B. L. (1976). Spatial distribution of earthquakes and subduction of the Nazca plate beneath South America. *Geology*, 4(11), 686–692. https://doi.org/10.1130/0091-7613(1976)4<686:SDOEAS>2.0.CO;2
- Bostock, M. G., Hyndman, R. D., Rondenay, S., & Peacock, S. M. (2002). An inverted continental Moho and serpentinization of the forearc mantle. *Nature*, 417(6888), 536–538. https://doi.org/10.1038/417536a
- Burd, A. I., Booker, J. R., & Mackie, R. (2013). Electrical conductivity of the Pampean shallow subduction region of Argentina near 33 S: Evidence for a slab window. *Geochemistry, Geophysics, Geosystems, 14*, 3192–3209. https://doi.org/10.1002/ggge.20213/pdf
- Cahill, T., & Isacks, B. (1992). Seismicity and shape of the subducted Nazca plate. *Journal of Geophysical Research*, 97, 17,503–17,529. https://doi.org/10.1029/92JB00493
- Cloos, M. (1993). Lithospheric buoyancy and collisional orogenesis: Subduction of oceanic plateaus, continental margins, island arcs, spreading ridges, and seamounts. *Geological Society of America Bulletin*, 105, 715. https://doi.org/10.1130/0016-7606(1993)105<0715: LBACOS>2.3.CO:2
- Cross, T. A., & Pilger, R. Jr. (1982). Controls of subduction geometry, location of magmatic arcs, and tectonics of arc and back-arc regions. Geological Society of America Bulletin, 93(6), 545. https://doi.org/10.1130/0016-7606(1982)93<545:COSGLO>2.0.CO;2
- DeMets, C., Gordon, R. G., & Argus, D. F. (2010). Geologically current plate motions. *Geophysical Journal International*, 181(1), 1–80. https://doi.org/10.1111/j.1365-246X.2009.04491.x
- Dickinson, W. R., & Snyder, W. S. (1978). Plate tectonics of the. *Laramide Orogeny*, 151, 355–366. https://doi.org/10.1130/MEM151-p355 Dueker, K. G., & Sheehan, A. F. (1997). Mantle discontinuity structure from midpoint stacks of converted P to S waves across the Yellowstone hotspot track. *Journal of Geophysical Research*, 102, 8313–8327. https://doi.org/10.1029/96JB03857
- English, J. M., Johnston, S. T., & Wang, K. (2003). Thermal modelling of the Laramide orogeny: Testing the flat-slab subduction hypothesis. Earth and Planetary Science Letters, 214(3–4), 619–632. https://doi.org/10.1016/S0012-821X(03)00399-6
- Farra, V., & Vinnik, L. (2000). Upper mantle stratification by P and S receiver functions. *Geophysical Journal International*, 141(3), 699–712. Ford, H. A., Long, M. D., & Wirth, E. A. (2016). Mid-lithospheric discontinuities and complex anisotropic layering in the mantle lithosphere beneath the Wyoming and superior provinces. *Journal of Geophysical Research: Solid Earth*, 121, 6675–6697. https://doi.org/10.1002/
- French, S. W., & Romanowicz, B. (2015). Broad plumes rooted at the base of the Earth's mantle beneath major hotspots. *Nature*, 525(7567), 95–99. https://doi.org/10.1038/nature14876
- Fromm, R., Alvarado, P., Alvarado, P. M., Beck, S. L., & Zandt, G. (2006). The April 9, 2001 Juan Fernandez Ridge (Mw 6.7) Tensional Outer-Rise Earthquake and its Aftershock Sequence. *Journal of Official Statistics*, 10(2), 163–170. https://doi.org/10.1007/s10950-006-9013-3
- Fromm, R., Zandt, G., & Beck, S. L. (2004). Crustal thickness beneath the Andes and Sierras Pampeanas at 30 S inferred from Pn apparent phase velocities. *Geophysical Research Letters*, 31, L06625. https://doi.org/10.1029/2003GL019231
- Gans, C. R., Beck, S. L., Zandt, G., Gilbert, H., Alvarado, P. M., Alvarado, P., et al. (2011). Continental and oceanic crustal structure of the Pampean flat slab region, western Argentina, using receiver function analysis: New high resolution results. *Geophysical Journal International*. 186(1), 45–58. https://doi.org/10.1111/j.1365-246X.2011.05023.x
- Gilbert, H. J., Beck, S., & Zandt, G. (2006). Lithospheric and upper mantle structure of Central Chile and Argentina. *Geophysical Journal International*, 165(1), 383–398. https://doi.org/10.1111/j.1365-246X.2006.02867.x
- Gutscher, M. A. (2002). Andean subduction styles and their effect on thermal structure and interplate coupling. *Journal of South American Earth Sciences*, 15(1), 3–10. https://doi.org/10.1016/S0895-9811(02)00002-0
- Gutscher, M.-A., Maury, R., Eissen, J. P., & Bourdon, E. (2000). Can slab melting be caused by flat subduction? *Geology*, 28(6), 535. https://doi.org/10.1130/0091-7613(2000)28<535:CSMBCB>2.0.CO;2
- Gutscher, M. A., Spakman, W., Bijwaard, H., & Engdahl, E. R. (2000). Geodynamics of flat subduction: Seismicity and tomographic constraints from the Andean margin. *Tectonics*, 19, 814–833. https://doi.org/10.1029/1999TC001152
- Hacker, B. R., Peacock, S. M., Abers, G. A., Abers, G. A., & Holloway, S. D. (2003). Subduction factory 2. Are intermediate-depth earthquakes in subducting slabs linked to metamorphic dehydration reactions. *Journal of Geophysical Research*, 108(B1), 2030. https://doi.org/10.1029/ 2001JB001129
- Hansen, S., & Dueker, K. (2009). P- and S-wave receiver function images of crustal imbrication beneath the Cheyenne Belt in southeast Wyoming P- and S-wave receiver function images of crustal imbrication beneath the Cheyenne Belt. *Bulletin of the Seismological Society of America*. 99(3), 1953–1961. https://doi.org/10.1785/0120080168
- Hansen, S. M., Dueker, K., & Schmandt, B. (2015). Thermal classification of lithospheric discontinuities beneath USArray. *Earth and Planetary Science Letters*, 431(C), 36–47. https://doi.org/10.1016/j.epsl.2015.09.009
- Hayes, G. P., Wald, D. J., & Johnson, R. L. (2012). Slab1.0: A three-dimensional model of global subduction zone geometries. *Journal of Geophysical Research*, 117, B01302. https://doi.org/10.1029/2011JB008524
- Heit, B., Yuan, X., Bianchi, M., Sodoudi, F., & Kind, R. (2008). Crustal thickness estimation beneath the southern Central Andes at 30 S and 36 S from S wave receiver function analysis. *Geophysical Journal International*, 174(1), 249–254. https://doi.org/10.1111/j.1365-246X.2008.03780.x



- Helffrich, G. (2006). Extended-time multitaper frequency domain cross-correlation receiver-function estimation. *Bulletin of the Seismological Society of America*, 96(1), 344–347. https://doi.org/10.1785/0120050098
- Hu, J., & Liu, L. (2016). Abnormal seismological and magmatic processes controlled by the tearing South American flat slabs. *Earth and Planetary Science Letters*, 450(C), 40–51. https://doi.org/10.1016/j.epsl.2016.06.019
- Jischke, M. C. (1975). On the dynamics of descending lithospheric plates and slip zones. *Journal of Geophysical Research*, 80, 4809–4813. https://doi.org/10.1029/JB080i035p04809
- Jordan, T. E., Allmendinger, R. W., & Allmendinger, R. W. (1986). The Sierras Pampeanas of Argentina: A modern analogue of Rocky Mountain foreland deformation. *The American Journal of the Medical Sciences*, 286(10), 737–764. https://doi.org/10.2475/aic.286.10.737
- Jordan, T. E., Isacks, B. L., Allmendinger, R. W., Allmendinger, R. W., Brewer, J. A., Ramos, V. A., et al. (1983). Andean tectonics related to geometry of subducted Nazca plate. *Geological Society of America Bulletin*, *94*(3), 341. https://doi.org/10.1130/0016-7606(1983)94<341: ATRTGO>2.0.CO:2
- Kay, S. M., & Abbruzzi, J. M. (1996). Magmatic evidence for Neogene lithospheric evolution of the central Andean. *Tectonophysics*, 259(1–3), 15–28. https://doi.org/10.1016/0040-1951(96)00032-7
- Kay, S. M., & Mpodozis, C. (2002). Magmatism as a probe to the Neogene shallowing of the Nazca plate beneath the modern Chilean flat-slab. Journal of South American Earth Sciences, 15(1), 39–57. https://doi.org/10.1016/S0895-9811(02)00005-6
- Kennett, B. L. N., & Engdahl, E. R. (1991). Traveltimes for global earthquake location and phase identification. *Geophysical Journal International*, 105(2), 429–465. https://doi.org/10.1111/j.1365-246X.1991.tb06724.x
- Kopp, H., Flueh, E. R., Papenberg, C., & Klaeschen, D. (2004). Seismic investigations of the O'Higgins Seamount Group and Juan Fernandez ridge: Aseismic ridge emplacement and lithosphere hydration. *Tectonics*, 23, TC2009. https://doi.org/10.1029/2003TC001590
- Kumar, P., Kind, R., Hanka, W., Wylegalla, K., Reigber, C., Yuan, X., et al. (2005). The lithosphere-asthenosphere boundary in the North-West Atlantic region. Earth and Planetary Science Letters, 236(1–2), 249–257. https://doi.org/10.1016/j.epsl.2005.05.029
- Leeds, A. R. (1975). Lithospheric thickness in the western Pacific. *Physics of the Earth and Planetary Interiors*, 11(1), 61–64. https://doi.org/10.1016/0031-9201(75)90075-8
- Lekić, V., & Fischer, K. M. (2014). Contrasting lithospheric signatures across the western United States revealed by Sp receiver functions. *Earth and Planetary Science Letters*, 402, 90–98. https://doi.org/10.1016/j.epsl.2013.11.026
- Li, X., Kind, R., Yuan, X., Lbern, I. W., & Hanka, W. (2004). Rejuvenation of the lithosphere by the Hawaiian plume. *Nature*, 427(6977), 827–829. https://doi.org/10.1038/nature02349
- Linkimer, L. (2011), Lithospheric structure of the Pampean Flat Slab (latitude 30–33S) and Northern Costa Rica (latitude 9–11N) subduction zones, University of Arizona, Tucson.
- Liu, L., & Gao, S. S. (2018). Lithospheric layering beneath the contiguous United States constrained by S-to-P receiver functions. *Earth and Planetary Science Letters*, 495, 79–86. https://doi.org/10.1016/j.epsl.2018.05.012
- Liu, L., Gurnis, M., Seton, M., Saleeby, J., Ller, R. D. M., & Jackson, J. M. (2010). The role of oceanic plateau subduction in the Laramide orogeny. Nature Geoscience, 3(5), 353–357. https://doi.org/10.1038/ngeo829
- Lynner, C., Anderson, M. L., Portner, D. E., Beck, S. L., & Gilbert, H. (2017). Mantle flow through a tear in the Nazca slab inferred from shear wave splitting. *Geophysical Research Letters*, 44, 6735–6742. https://doi.org/10.1002/2017GL074312
- Ma, Y., & Clayton, R. W. (2015). Flat slab deformation caused by interplate suction force. *Geophysical Research Letters*, 42, 1–9. https://doi.org/10.1002/(ISSN)1944-8007
- Manea, V., & Gurnis, M. (2007). Subduction zone evolution and low viscosity wedges and channels. Earth and Planetary Science Letters, 264(1–2), 22–45. https://doi.org/10.1016/j.epsl.2007.08.030
- Manea, V. C., Pèrez-Gussinyè, M., & Manea, M. (2011). Chilean flat slab subduction controlled by overriding plate thickness and trench roll-back. *Geology*, 40(1), 35–38. https://doi.org/10.1130/G32543.1
- Montelli, R., Nolet, G., Dahlen, F. A., & Masters, G. (2006). A catalogue of deep mantle plumes: New results from finite-frequency tomography. *Geochemistry, Geophysics, Geosystems, 7*, Q11007. https://doi.org/10.1029/2006GC001248
- Müller, R. D., Sdrolias, M., Gaina, C., & Roest, W. R. (2008). Age, spreading rates, and spreading asymmetry of the world's ocean crust. *Geochemistry, Geophysics, Geosystems*, 9, Q04006. https://doi.org/10.1029/2007GC001743
- Obrebski, M., Allen, R. M., Xue, M., & Hung, S.-H. (2010). Slab-plume interaction beneath the Pacific Northwest. *Geophysical Research Letters*, 37, L14305. https://doi.org/10.1029/2010GL043489
- O'Driscoll, L. J., Humphreys, E. D., & Saucier, F. (2009). Subduction adjacent to deep continental roots: Enhanced negative pressure in the mantle wedge, mountain building and continental motion. *Earth and Planetary Science Letters*, 280(1–4), 61–70. https://doi.org/10.1016/j.epsl 2009 01 020
- Park, J., & Levin, V. (2000). Receiver functions from multiple-taper spectral correlation estimates. Bulletin of the Seismological Society of America, 90(6), 1507–1520. https://doi.org/10.1785/0119990122
- Phillips, K., & Clayton, R. W. (2014). Structure of the subduction transition region from seismic array data in southern Peru. *Geophysical Journal International*, 196(3), 1889–1905. https://doi.org/10.1093/gjj/ggt504
- Pilger, R. E. X. H. Jr. (1981). Plate reconstructions, aseismic ridges, and low-angle subduction beneath the Andes. *Geological Society of America Bulletin*, 92(7), 448. https://doi.org/10.1130/0016-7606(1981)92<448:PRARAL>2.0.CO;2
- Porter, R., Gilbert, H., Zandt, G., Beck, S., Warren, L., Calkins, J., et al. (2012). Shear wave velocities in the Pampean flat-slab region from Rayleigh wave tomography: Implications for slab and upper mantle hydration. *Journal of Geophysical Research*, 117, B11301. https://doi.org/10.1029/2012JB009350
- Portner, D. E., Beck, S., Zandt, G., & Scire, A. (2017). The nature of subslab slow velocity anomalies beneath South America. *Geophysical Research Letters*, 44, 4747–4755. https://doi.org/10.1002/2017GL073106
- Ramos, V. A. (2010). The Grenville-age basement of the Andes. *Journal of South American Earth Sciences*, 29(1), 77–91. https://doi.org/10.1016/i.jsames.2009.09.004
- Ramos, V. A., Cristallini, E. O., & Pérez, D. J. (2002). The Pampean flat-slab of the Central Andes. *Journal of South American Earth Sciences*, 15(1), 59–78.
- Scire, A., Zandt, G., Beck, S., Long, M., Wagner, L., Minaya, E., et al. (2015). Imaging the transition from flat to normal subduction: Variations in the structure of the Nazca slab and upper mantle under southern Peru and northwestern Bolivia. *Geophysical Journal International*, 204(1), 457–479. https://doi.org/10.1093/gji/ggv452
- Shibutani, T., Ueno, T., & Hirahara, K. (2008). Improvement in the extended-time multitaper receiver function estimation technique. *Bulletin of the Seismological Society of America*, 98(2), 812–816. https://doi.org/10.1785/0120070226
- Stern, R. J. (2002). Subduction zones. Reviews of Geophysics, 40(4), 1012. https://doi.org/10.1029/2001RG000108



- Tassara, A., & Echaurren, A. (2012). Anatomy of the Andean subduction zone: Three-dimensional density model upgraded and compared against global-scale models. *Geophysical Journal International*, 189(1), 161–168. https://doi.org/10.1111/j.1365-246X.2012.05397.x
- Tassara, A., Gotze, H. J., Schmidt, S., & Hackney, R. (2006). Three-dimensional density model of the Nazca plate and the Andean continental margin. *Journal of Geophysical Research*, 111, B09404. https://doi.org/10.1029/2005JB003976
- Uyeda, S., & Kanamori, H. (1979). Back-arc opening and the mode of subduction. *Journal of Geophysical Research*, 84, 1049–1061. https://doi.org/10.1029/JB084iB03p01049
- van Hunen, J., van den Berg, A. P., & Vlaar, N. J. (2002a). On the role of subducting oceanic plateaus in the development of shallow flat subduction. *Tectonophysics*, 352(3–4), 317–333. https://doi.org/10.1016/S0040-1951(02)00263-9
- van Hunen, J., van den Berg, A. P., & Vlaar, N. J. (2002b). The impact of the South-American plate motion and the Nazca Ridge subduction on the flat subduction below South Peru. Geophysical Research Letters, 29(14), 1690. https://doi.org/10.1029/2001GL014004
- van Hunen, J., van den Berg, A. P., & Vlaar, N. J. (2004). Various mechanisms to induce present-day shallow flat subduction and implications for the younger Earth: A numerical parameter study. *Physics of the Earth and Planetary Interiors*, 146(1–2), 179–194. https://doi.org/10.1016/j.pepi.2003.07.027
- Wessel, P., Smith, W. H. F., Scharroo, R., Luis, J., & Wobbe, F. (2013). Generic Mapping Tools: Improved Version Released, 94(45), 409–410. https://doi.org/10.1002/2013E0450001
- Wilson, D. C., Angus, D. A., Ni, J. F., & Grand, S. P. (2006). Constraints on the interpretation of S-to-P receiver functions. *Geophysical Journal International*, 165(3), 969–980. https://doi.org/10.1111/j.1365-246X.2006.02981.x
- Wirth, E. A., & Long, M. D. (2014). A contrast in anisotropy across mid-lithospheric discontinuities beneath the central United States—A relic of craton formation. *Geology*, 42(10), 851–854. https://doi.org/10.1130/G35804.1
- Yáñez, G. A., Cembrano, J., Pardo, M., Ranero, C., & Selles, D. (2002). The challenger-Juan Fernández-Maipo major tectonic transition of the Nazca-Andean subduction system at 33–34° S: Geodynamic evidence and implications. *Journal of South American Earth Sciences*, 15(1), 23–38. https://doi.org/10.1016/S0895-9811(02)00004-4
- Yáñez, G. A., Ranero, C. R., von Huene, R., & Díaz, J. (2001). Magnetic anomaly interpretation across the southern Central Andes (32°–34°S): The role of the Juan Fernández Ridge in the late Tertiary evolution of the margin. *Journal of Geophysical Research*, 106, 6325–6345. https://doi.org/10.1029/2000JB900337
- Yuan, X., Kind, R., Li, X., & Wang, R. (2006). The S receiver functions: Synthetics and data example. *Geophysical Journal International*, 165(2), 555–564. https://doi.org/10.1111/j.1365-246X.2006.02885.x